applied sciences

MDPI

Article

A Comparison in the Use of the Crystallographic Structure of the Human A_1 or the A_{2A} Adenosine Receptors as a Template for the Construction of a Homology Model of the A_3 Subtype

Enrico Margiotta and Stefano Moro *

Molecular Modeling Section (MMS), Dipartimento di Scienze del Farmaco, Università di Padova, via Marzolo 5, 35131 Padova, Italy; enrico.margiotta@phd.unipd.it

* Correspondence: stefano.moro@unipd.it

Received: 30 January 2019; Accepted: 21 February 2019; Published: 26 February 2019

Featured Application: Molecular modelling, drug discovery, structure-based drug design, virtual screening, docking simulations and molecular dynamics simulations.

Abstract: In the last decades, the field of therapeutic application in targeting the human A_3 adenosine receptor has represented a rapidly growing area of research in adenosine field. Both agonists and antagonists have been described to have a potential application in the treatment of several diseases, including, for example, glaucoma, cancer, and autoimmune inflammations. To date, the most severe factor limiting the accuracy of the structure-based molecular modeling approaches is the fact that the three-dimensional human A_3 structure has not yet been solved. However, the crystallographic structures of either human A_1 or A_{2A} subtypes are available as potential templates for the construction of its homology model. In this study, we have compared the propensity of both models to accommodate a series of known potent and selective human A_3 agonists and antagonists. As described, on the basis of the results obtained from this preliminary study, it is possible to affirm that the human A_3 receptor model based on the crystallographic structure of the A_1 subtype can represent a valid alternative to the one conventionally used today, based on the available A_{2A} structures.

Keywords: G protein-coupled receptor; adenosine receptors; A_3 adenosine receptor; homology modeling; molecular docking; structure-activity relationship

1. Introduction

Adenosine is a key extracellular signaling molecule that regulates the cellular responses to tissue damage, hypoxia, and energy depletion, through activation of G protein-coupled receptors [1]. To date, four adenosine receptor (AR) subtypes have been identified and pharmacologically characterized: A_1 A_{2A}, A_{2B}, and A_3. These receptors are ubiquitously expressed on almost all cell types [1]. Retrospectively, the human A_3 AR subtype (hA_3 AR) was the last member of the adenosine family to have been cloned. It was originally described in 1991 by Meyerhof and collaborators as an orphan receptor from rat testis and coded as tgpcr1, sharing 40% of sequence similarity with canine A_1 and A_{2A} ARs [2]. One year later, Zhou and collaborators described the cDNA sequence, initially named R226 and extracted from the rat striatum, that encoded for a G protein-coupled receptor with an identical sequence of tgpcr1 and able to bind adenosine [3]. This experimental evidence led to the conclusion that it was a new AR subtype, namely A_3. In the last decades, the field of the therapeutic application in targeting the hA_3 AR represents a rapidly growing area of research in adenosine field, both agonists and antagonists have been described to have a potential application in the treatment of several diseases, e.g. glaucoma, cancer,

and autoimmune inflammations [4]. In particular, hA_3 AR agonists have been recently described as promising antinociceptive agents in different preclinical models of chronic pain [5] and in clinical trials as drug candidates for treating psoriasis, rheumatoid arthritis, and hepatocellular carcinoma [6]. In addition, hA_3 AR antagonists were described as potential drug candidates for the treatment of respiratory tract inflammations, such as asthma [7] and glaucoma [8].

As recently reviewed by several authors, in the recent past structure-based molecular modeling approaches, above all molecular docking, have been increasingly applied in rationalizing the structure-activity relationships (SARs) of both agonists and antagonists and in supporting the design of novel potent and selective hA_3 AR ligands [9]. More recently, molecular dynamics (MD) simulations have been performed to elucidate the ligand recognition at the hA_3 AR [10].

To date, the most severe fact that limits the accuracy of the structure-based molecular modeling approaches is due to the fact that the three-dimensional hA_3 AR structure has not been solved yet. The first fundamental breakthrough in this field is the disclosure of the first structure of the hA_{2A} AR, a close homolog, which allowed the construction of three-dimensional models for homology by an accuracy level much higher than before, in terms of sequence identity and resolution of the available templates [11]. Following the publication of the first structure, the availability of novel crystallographic information of hA_{2A} AR in complexes with both agonists and antagonists are contributing to increase the knowledge at the molecular level of ligand recognition at ARs, leading, finally, to an increased applicability domain and accuracy of structure-based ligand design (SBLD) approaches (not only in the adenosine field). Nowadays, just 46 crystal structures are already available, bound to a wide variety of agonists and antagonists that are either natural or synthetic, and representing the majority of structural determinants on adenosine receptors ligands' activity. However, dealing with the hA_3 AR at a molecular level is still challenging, because the accuracy of the hA_3 AR model strongly depends on the sequence identity/similarity and resolution of the available crystallographic templates used for its construction. These bioinformatics and structural details are particularly important especially if we consider their impact in guaranteeing an accurate structural description of extra-cellular domains, for which it has already been described as having a key role in defining both the ligand orthosteric binding site and the ligand meta-binding sites [12–14].

Very recently, crystallographic structures of the hA_1 AR have been solved, representing both its active [15] and inactive conformation [16]. These structures were co-crystallized with the endogenous agonist adenosine (PDB code: 6D9H), as with the antagonist 4-{[3-(8-cyclohexyl-2,6-dioxo-1-propyl-1,2,6,7-tetrahydro-3H-purin-3-yl)propyl]carbamoyl}benzene-1-sulfonyl fluoride (PDB code: 5UEN), which actually constitutes the most representative example of an interaction scheme for the system of interest.

As expected, several remarkable differences to the previously solved hA_{2A} AR structures have been underlined, in particular, the hA_1 AR revealed a peculiar conformation of the second extracellular loop and a wider ligand binding site (Figure 1). Intriguingly, from a phylogenetic and functional point of view, the hA_3 AR is much closer to the hA_1 AR than to the hA_{2A} AR. Indeed, hA_3 AR shows a higher sequence identity with the hA_1 AR (54%) than the hA_{2A} AR (49%), and both A_3 AR and A_1 AR, coupled to $G_{i/o}$ proteins share, from a functional point of view, the crucial biochemical pathway based on the inactivation of the adenyl cyclase activity. Structurally, another important element of similarity between the hA_3 AR and the hA_1 AR is related to both receptors having only a single cysteine residue on the second extracellular loop (EL2) which establishes a disulfide bridge, largely conserved among the Rhodopsin-family of GPCRs, along with a second cysteine located on the transmembrane helix 3 (TM3) [15,16]. Moreover, the lack of the additional disulfide bridges at the EL2 level, as present in the A_{2A} AR subtype, involves a significant reorganization of the transmembrane helices 1, 2, 3 and 7, leading to a different shape of the orthosteric binding cavity. An additional disulfide, C260-C263, present in both A_1 AR and A_{2A} AR, staples the conformation of the EL3.

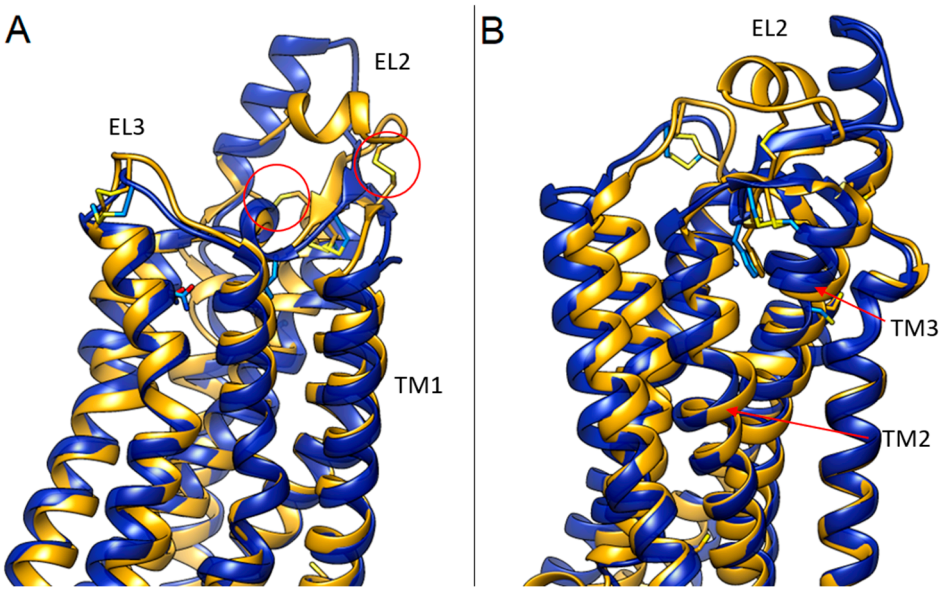

Figure 1. Structural superposition of hA_1 (dark blue) and hA_{2a} (gold) ARs crystal structures in their active state (PDB code: 6D9H and 2YDO, respectively). Panel (**A**) and (**B**) representations differ only for camera orientation. Additional A_{2A} disulfide bridges are highlighted in red.

Taking all the above arguments into consideration, from a computational point of view the question arises spontaneously: "could the crystallographic structure of the human A_1 AR be a better template than the human A_{2A} AR for the construction of a homology model of the A_3 subtype?", the question which provided the scientific motivation in taking up the present research work. To appreciate the qualitative and the quantitative differences obtained by using the two alternative templates, we decided to retrospectively compare the posing and scoring performance of molecular docking for a selection of well-known potent selective agonists and antagonists, summarized in Figures 2 and 3.

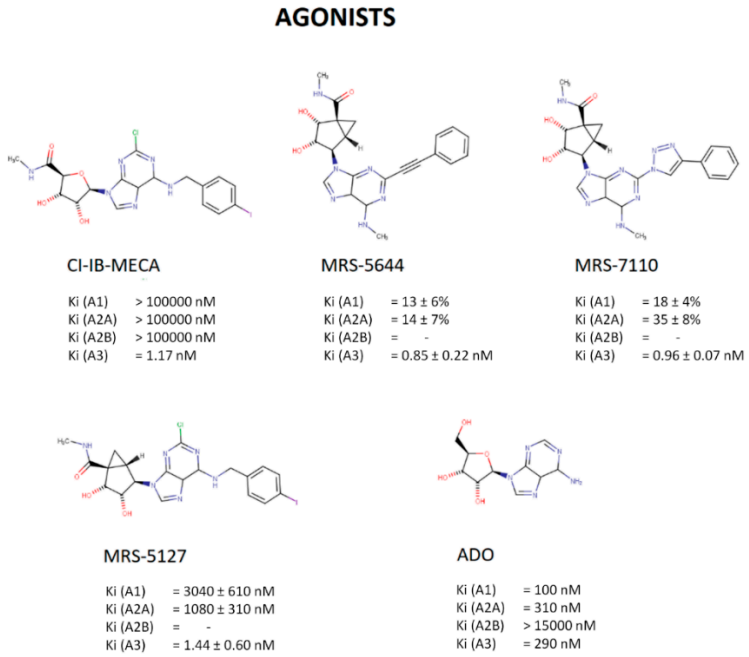

Figure 2. Chemical structures of agonists selected for docking studies. Experimental Ki values (in nM or activity assay percentages) for each receptor subtype are also reported for comparison.

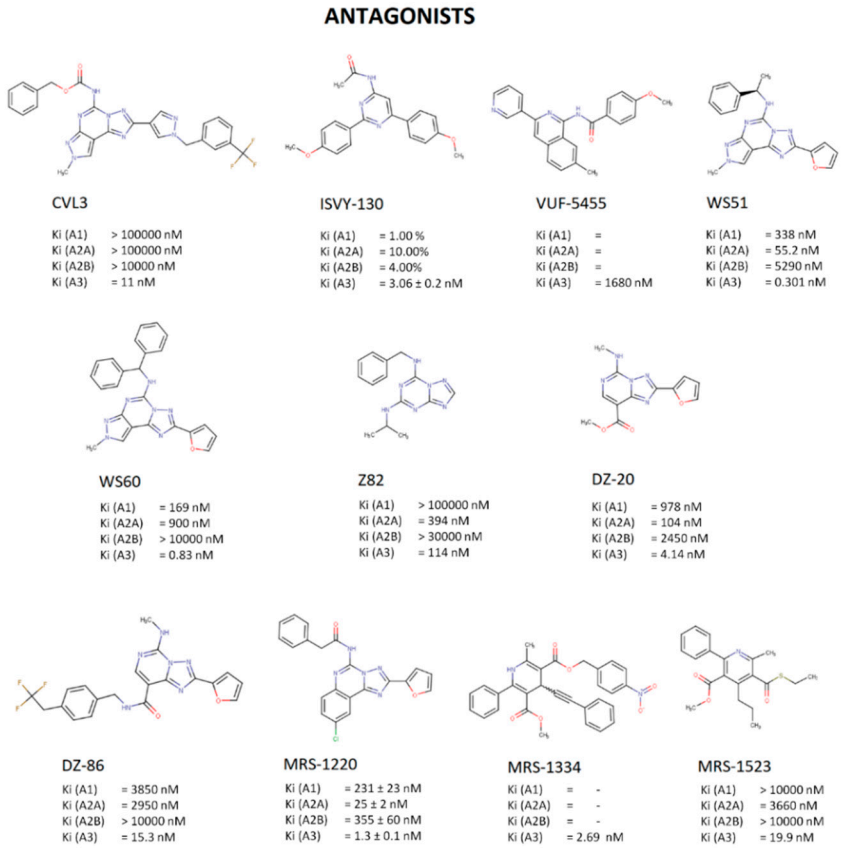

Figure 3. Chemical structures of antagonists selected for docking studies. Experimental Ki values (in nM or activity assay percentages) for each receptor subtype are also reported for comparison.

2. Materials and Methods

2.1. Computational Facilities

The MOE suite (Molecular Operating Environment, version 2016.0801) [17] was exploited to perform general molecular modeling operations. All computations were carried out on a 12 CPU (Intel®Xeon®CPU E5-1650 3.80GHz) Linux workstation (distribution 14.04, 64 bit). Docking simulations were performed exploiting the docking program GOLD 5.4.1 [18] and the Scoring Function GoldScore. Plots were generated using Gnuplot 4.6 [19]. 2D chemical structures were drawn with Marvin Sketch [20]. Molecular graphics were performed with the UCSF Chimera package [21].

2.2. Protein Preparation

The hA_{2A} and hA_1 AR crystallographic structures were retrieved from the RCSB Protein Data Bank (PDB) database [22]. In the case of inactive models, the A_3-3PWH model was retrieved from the *Adenosiland* web-platform [23]. Fusion proteins and antibody portions were removed, along with ions and any other co-crystallized molecule. Protein structures were ionized using MOE Protonate 3D tool [24], at physiological pH 7.4, temperature 310 K and salt concentration 0.1 M. The Generalized Born (GB) solvation model [25] was used, with an inner dielectric constant value of 2 and the 800 R3 van der Waals (vdW) energy function. MOE energy minimization tool was exploited to minimize contacts between hydrogen atoms, using the Amber12:EHT force field [26], until the RMS of the conjugate gradient was < 0.05 kcal·mol^{-1}·Å^{-1}. Sodium ion and its first hydration shell were included during docking simulations on antagonists, basing on one of the highest resolution hA_{2A} AR crystal structures: PDB code 5NM2 [27]. The 3D-structures of ligands were built by the MOE-builder tool. Tautomeric states and atoms' hybridization were checked. Geometry minimization was performed

by the MMFF94x [28], setting the root mean square gradient < 0.05 kcal·mol^{-1}·Å^{-1}. Ligands partial charges were calculated by means of the PM3/ESP semiempirical Hamiltonian [29]. Protein atomic partial charges were computed according to the Amber12:EHT force field.

2.3. Sequence Alignment

The hA_1 and hA_{2A} AR crystallographic structures (5UEN and 3PWH, respectively) were aligned and superposed by MOE Sequence Editor. Structural domains were annotated basing on visual inspection of each TM region. The canonical fasta sequence of the hA_3 adenosine receptor (ID P0DMS8-1) was retrieved from the UniProt database [30] and aligned on the sequences of hA_1 and hA_{2A} AR (see Table 1). Sequence identity and similarity percentages were calculated for all domains using BLOSUM62 matrix (see Results section). To perform a more robust comparative analysis, we calculated the deviation values between either sequence identity (SI) or sequence similarity (SS) of each domain of the hA_3 AR calculated on the hA_1 (A3/A1) from the one calculated on the hA_{2A} AR (A3/A2a), as reported in Equations (1) and (2):

$$\Delta SI = \frac{(SI_{A3/A1} - SI_{A3/A2a})}{SI_{min_{(A1,A2a)}}} \cdot 100 \quad (1)$$

$$\Delta SS = \frac{(SS_{A3/A1} - SS_{A3/A2a})}{SS_{min_{(A1,A2a)}}} \cdot 100 \quad (2)$$

Negative values are in favor of the hA_{2A} subtype, while positive values are of hA_1.

Table 1. Sequence alignment of the hA3 AR canonical isoform primary sequence (second row) on the PDB crystallographic structures 5UEN (hA_1 AR) and 3PWH (hA_{2A} AR), basing on respective structural domains.

	A3/A1 Sequence Alignment	A3/A2A Sequence Alignment
TM1	^{10}AAYIGIEVLIALVSVPGNVLVIWAVKV^{36} ^{13}VTYITMEIFIGLCAIVGNVLVICVVKL^{39}	^{15}AIAVLAILGNVLVCWAVWLNSNLQNVT^{41} ^{21}FIGLCAIVGNVLVICVVKLNPSLQTTT^{47}
IL1	^{37}NQALRD^{42} ^{40}NPSLQT^{45}	^{42}NYFVVS^{47} ^{48}FYFIVS^{53}
TM2	^{43}ATFCFIVSLAVADVAVGALVIPLAILINI^{71} ^{46}TTFYFIVSLALADIAVGVLVMPLAIVVSL^{74}	^{48}LAAADIAVGVLAIPFAITISTGFCAACHG^{76} ^{54}LALADIAVGVLVMPLAIVVSLGITIHFYS^{82}
EL1	^{72}GPQTY^{76} ^{75}GITIH^{79}	^{77}CLFIA^{81} ^{83}CLFMT^{87}
TM3	^{77}FHTCLMVACPVLILTQSSILALLAIAVDRYLRVK^{110} ^{80}FYSCLFMTCLLLIFTHASIMSLLAIAVDRYLRVK^{13}	^{82}CFVLVLTQSSIFSLLAIAIDRYIAIRIPLRYNGL^{115} ^{88}CLLLIFTHASIMSLLAIAVDRYLRVKLTVRYKRV^{121}
IL2	^{111}IPLRYKMVVT^{120} ^{114}LTVRYKRVTT^{123}	^{116}VTGTRAKGII^{125} ^{122}TTHRRIWLAL^{131}
TM4	^{121}PRRAAVAIAGCWILSFVVGLTPMF^{144} ^{124}HRRIWLALGLCWLVSFLVGLTPMF^{147}	^{126}AICWVLSFAIGLTPMLGWNNCGQP^{149} ^{132}GLCWLVSFLVGLTPMFGWNMKLTS^{155}
EL2	^{145}GWNNLSAVERAWAANGSMGEPVIKCEFEKVIS^{176} ^{148}GWNMKLTSE–YHRNVTF—-LSCQFVSVMR^{173}	^{150}KEGKNHSQGCGEGQVACLFEDVVP^{173} ^{156}EYHRNVTFLSCQFVSVMR^{173}——
TM5	^{177}MEYMVYFNFFVWVLPPLLLMVLIYLEVFYLIRKQ^{210} ^{174}MDYMVYFSFLTWIFIPLVVMCAIYLDIFYIIRNK^{207}	^{174}MNYMVYFNFFACVLVPLLLMLGVYLRIFLAARRQ^{207} ^{174}MDYMVYFSFLTWIFIPLVVMCAIYLDIFYIIRNK^{207}
IL3	^{211}LNKKVSASSGDPQ^{223} ^{208}LSLNLS-NSKETG^{219}	^{208}LKQMESQPLPGERAR^{222} ^{208}LSLNLSN—SKETG^{219}
TM6	^{224}KYYGKELKIAKSLALILFLFALSWLPLHILNCITLF^{259} ^{220}AFYGREFKTAKSLFLVLFLFALSWLPLSIINCIIYF^{255}	^{223}STLQKEVHAAKSLAIIVGLFALCWLPLHIINCFTFF^{258} ^{220}AFYGREFKTAKSLFLVLFLFALSWLPLSIINCIIYF^{255}
EL3	^{260}CPSCHKP^{266} —-^{256}NGEVP^{260}	^{259}CPDCSHAP^{266} ^{256}N—GEVP^{260}
TM7	^{267}SILTYIAIFLTHGNSAMNPIVYAFR^{291} ^{261}QLVLYMGILLSHANSMMNPIVYAYK^{285}	^{267}LWLMYLAIVLSHTNSVVNPFIYAYR^{291} ^{261}QLVLYMGILLSHANSMMNPIVYAYK^{285}

2.4. Homology Modeling

Homology models of both the active and the inactive state were built using the MOE Homology Model Tool. Only aligned residues were overridden. C/N-terminus outgap modeling was disabled, while automatic detection of disulfide bonds was enabled. The maximum number of main chain models was set to 10 and side chain sampling was set to 1 at 300 K. Differently from the intermediates, the final state was ionized at physiological pH (7.4 units) and subjected to medium minimization in order to moderately relieve the steric strain, according to the AMBER12:EHT force field. The final output model was checked, inspecting the wellness of its assigned biophysical parameters and scores, along with good superposition with the reference structure, transmembrane domain side chain rotamers and exposure, dissociation state of charged residues and tautomeric state of the histidine residues. For inactive state model of the hA_3 AR, the following template *PDB* structures were adopted and then subjected to the comparison (see Section 3): 3PWH, 5NM2 (A_{2a}) and 5UEN (A_1). For the active state model 2YDO (A_{2A}-based) and 6D9H (A_1-based) PDB templates were used. All generated homology models passed with all major biophysical checkpoints, basing on the MOE tool. For the adenosine bound hA_1 AR crystal structure (PDB code: 6D9H), two homology models were carried out by disabling or enabling the *Induced Fit* option, respectively. This option permits the side chains of the amino acids defining the ligand binding pocket to adapt their conformational position around the ligand during the construction of the homology model.

2.5. Agonists and Antagonists Selection

A specific subset of agonists and antagonists against hA_3 AR has been selected basing on their potency and selectivity profiles, maximizing as much as possible their chemical diversity [31–48]. The selected ligands are shown in Figures 2 and 3.

2.6. Molecular Docking

GOLD (Genetic Optimization for Ligand Docking, version 5.4.1) docking algorithm was selected as a conformational search program and Goldscore as a scoring function, referring to previous docking benchmark studies performed by our research group [49–51]. For any ligand, 20 docking simulation runs were performed on each receptor subtype, searching on a sphere of 20Å radius, centered on the sidechain nitrogen of the conserved $N^{6.55}$. The RMSD threshold for the conformational search was set to 1.0 Å, and 20 poses were collected.

2.7. Docking Analysis

Ligand and protein partial charges were calculated using the PM3 method and AMBER12EHT force field respectively. Then, overall electrostatic (Ele) and van der Waals (vdW) energy contributions to the binding energy were calculated by MOE, together with per residue electrostatic and hydrophobic interactions, giving the so-called "Interaction Energy Fingerprints" (IEF) [49]. The interactions of most relevant residues were reported in histograms, whose height is proportional to the strength of the interaction. All the plots were produced using GNUPLOT 4.6 [19].

2.8. Docking-based Homology Models' Comparison

To appreciate the qualitative and the quantitative differences derived by using the two alternative templates, we decided to retrospectively compare the performance of molecular docking in posing and scoring for a selection of known potent and selective either agonists or antagonists. For each ligand and each homology model, 20 docking poses were retained and the representative one has been selected using the combination of two conditions: (1) the best match in reproducing the two crucial and conserved ligand-receptor interactions (hydrogen-bond with $N^{6.55}$ and π-π stacking with F^{EL2}); (2) for all poses in agreement with the previous condition, the best combination of the force field-driven energetic Ele and vdW contributions.

The EM correlation coefficient (whose value ranges between -2 and 2) was recently implemented as a statistical tool to evaluate the correlation between two variables dependent on one or more of interest, and to estimate the commutative influence of the latter without statistical bias [52]. It quantifies simultaneously (Equation (3), Figure 4): if two variables (numerical results), x and y, have the same absolute value and the same sign (positive or negative); the sign of each variable ($sgnx$, $sgny$); the ratio between x and y ($|x/y|$). Here, we demonstrate that the EM coefficient can be solved as a function of the ratio x/y:

$$\begin{aligned} EM &= \frac{\sqrt{(|xy|)}(sgnxsgny) - \left[\left(\frac{|x|+|y|}{2}\right)(sgnx)\right]}{\left(\frac{|x|+|y|}{2}\right)} \\ &= \frac{-x\left(y-\sqrt{|xy|}\right)^2}{|xy|(|x|+|y|)} \\ &= (sgnxsgny)\left(\frac{2\sqrt{|x/y|}}{|x/y|+1} - sgny\right) \\ EM_{gauss} &= (sgnxsgny)e^{\left(\frac{-2N^2}{3}\right)} - (sgnx) \end{aligned} \tag{3}$$

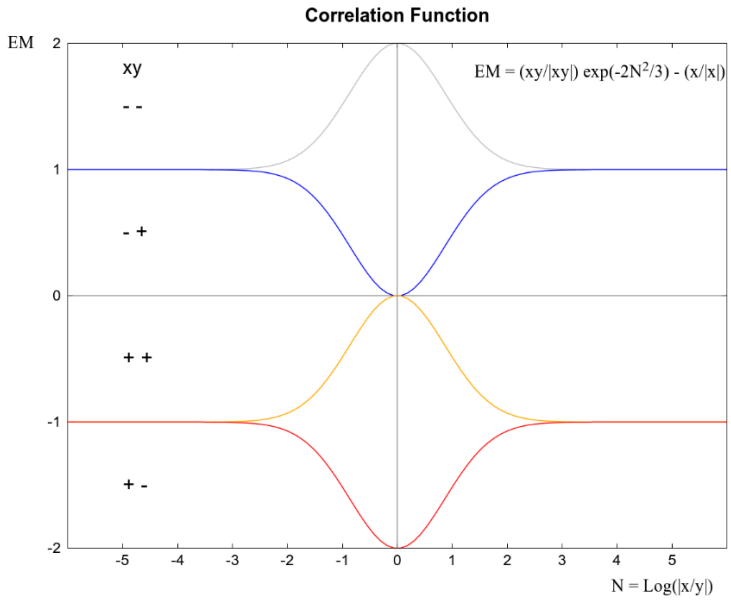

Figure 4. Graphical representation of the EM correlation coefficient (Equation (3)), a Gaussian function of the logarithmic ratio between x and y absolute values (N).

In this work, y, specifically, represents the energy contribution of the ligand (Ele or vdW) calculated on the reference model complex (A2a-based model), while x represents the energy contribution of the same ligand calculated on the model subjected to the comparison (A1-based model). Positive energy values indicate disfavored binding poses, negative values in contrast indicate favorable binding poses. Four combinations of x and y energy values are possible, giving four different possible behaviors:

1. one pose is better than the other (x model pose is better than y model pose, blue spots, −+; y model pose is better than x model pose, red spots, +−);
2. both the poses are disfavored (++, orange spots);
3. both the poses are favored (−−, white spots).

In the latter case of white spots, the exponential form of the EM coefficient is expressly related to the ratio of x and y, with a view to individuate the most favored pose. In this way, we determined the models' influence on the binding mode of ligands and, finally, their wellness.

2.9. MMSDocking Video Maker

The in-house MMsDocking video maker tool was exploited to produce videos showing the docking poses, per residue IEFhyd and IEFele data for selected residues. Representations of docking poses were produced using CHIMERA52 [21], two-dimensional depictions were constructed through the cheminformatics toolkit RDKit [52], the heat maps were obtained through GNUPLOT 4.6 [19]; in the end, videos were mounted using MEncoder [53].

3. Results and Discussion

3.1. Sequence Comparison and Homology Modeling

The bioinformatics analysis of the protein sequences of the four adenosine receptor subtypes has already been presented and discussed in the literature [54–56]. The overall sequence identity/similarity between human adenosine receptors is relatively high. Interestingly, the adenosine A_3 receptor reveals higher sequence identity/similarity to the adenosine A_1 receptor (48/69%) than to the adenosine A_{2A} (37/48%) receptor, as summarized in Tables 1 and 2.

Table 2. Sequence identity (SI) and sequence similarity (SS) percentages calculated for each alignment performed on structural domains of crystal structures 5UEN (hA_1 AR) and 3PWH (hA_{2A}). Overall values are also reported along with domains showing the highest SI and SS percentages.

	A3/A1		**A3/A2a**	
	SI(%)	**SS(%)**	**SI(%)**	**SS(%)**
TM1	48.1	66.7	51.9	63
IL1	33.3	66.7	66.7	83.3
TM2	65.5	89.7	51.7	62.1
EL1	20	40	60	80
TM3	64.7	85.3	47.1	76.5
IL2	50	70	20	30
TM4	58.3	79.2	50	66.7
EL2	25	40.6	12.5	25
TM5	52.9	79.4	44.1	67.6
IL3	23.1	58.3	13.3	20
TM6	69.4	80.6	50	66.7
EL3	14.3	28.6	12.5	12.5
TM7	52	76	48	80
overall	**48.2**	**68.7**	**31.6**	**47.8**
max	*TM6*	*TM2*	*IL1*	*IL1*

In homology modeling, the simplest template selection rule is to select the structure with the highest sequence similarity to the modeled sequence [57]. Moreover, when it is possible, a template bound to the same or similar ligands as the modeled sequence should generally be used. By the analysis of data shown in Table 2 and Figure 5, i.e., the SI% and SS% for all the receptor domains involved in the recognition of agonists and antagonists, the hA_1 AR can be considered a better possible template than the hA_{2A} AR.

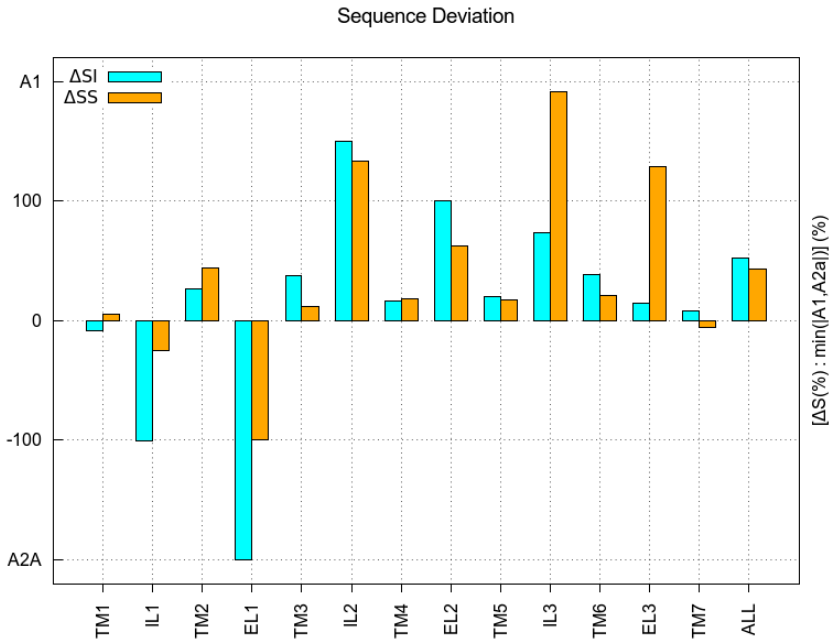

Figure 5. Sequence comparison calculations on each topological position and overall alignment. The percentage reported on the *y*-axis indicates how much the difference in identity (ΔSI, cyan), or in similarity (ΔSS, orange), favors alignment towards the hA1 or hA2a AR.

As anticipated in the Introduction, the A_3 AR has not yet been crystallized. To appreciate the qualitative and the quantitative differences derived by using hA_1 AR as alternative templates of the conventional hA_{2A} AR, we decided to retrospectively compare the performance of molecular docking in posing and scoring a selection of known potent and selective agonists and antagonists, summarized in Figures 2 and 3. Moreover, we have recently reported that the presence of the sodium ion and its first sphere of hydration improves the accuracy and precision of positioning of the antagonist, with respect to the crystallographic poses. This occurs through most of the docking programs and regardless of the chemical nature of the ligand [51]. These data are strongly consistent with the crystallographic evidence which would seem to indicate sodium and his first hydration sphere being an integral part of the orthosteric site that recognizes the structure of antagonist, even for those crystallographic structures in which these have not been solved. By logical extension, sodium and its first hydration sphere should be incorporated into all docking studies, taking into account the interaction between an antagonist and its orthosteric receptor cavity. On the contrary, the presence of sodium and its first hydration sphere, as observed crystallographically, are not an integral part of the orthosteric site that recognizes the structure of the agonist. Taking into account the evidence described above, in this work we have constructed two different hA_3 AR homology models: one used for the recognition of agonists (in which the sodium cation and its first hydration sphere are absent), and another used for the recognition of antagonists (in which the sodium cation and its first hydration sphere are an integral part of the orthostatic site).

3.2. *"Agonist-driven" hA_3 AR Models*

The first comparative validation was performed using the structure of adenosine, its endogenous agonist. We have compared the adenosine binding motif in both hA_1 AR and hA_{2A} AR crystallographic structures with those obtained through our docking procedure on the hA_3 AR models derived from the use of the two different crystallographic templates, hA_1 AR and hA_{2A} AR respectively. As shown in Figure 6, the best docking poses of adenosine in both the hA_3 ARs are geometrically similar to the crystallographic poses in hA_1 AR and hA_{2A} AR. In particular, in each model, adenosine engages

its canonical stabilizing bidentate H-bond of N7 and N^6 H with Asn250 (6.55) and the π-π stacking interaction with Phe168 (EL2).

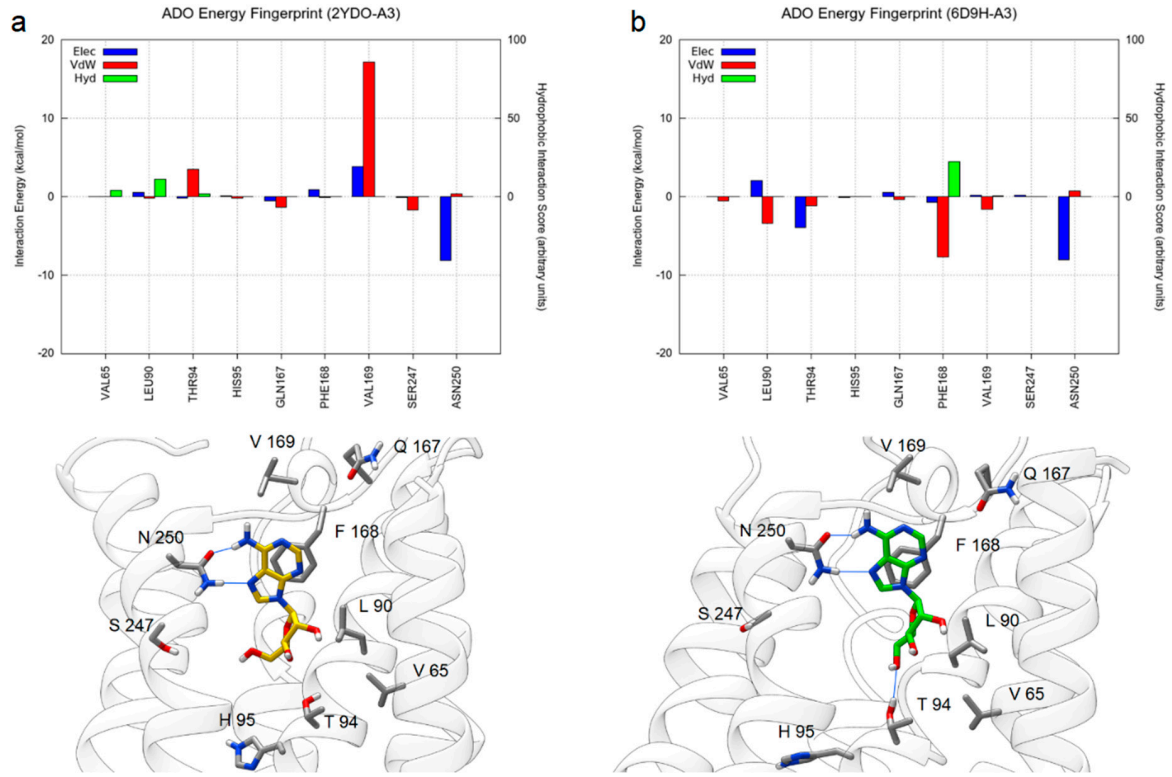

Figure 6. Per residue energy histograms and selected docking pose of adenosine on either the hA_{2A} based model (**a**) or the induced fit hA_1-based model (**b**).

However, in the case of the hA_{2A} AR model, the ribose ring is not anchored to Thr94 (3.36) by hydrogen bond, conversely, in the hA_1 AR model, it is, by a pretty network. This is also confirmed by corresponding energy histograms, in which the hA_{2A} AR model is shown to be highly disfavored not only because of Thr94 (3.36) but also of critical residues such as Val169 (EL2). Moreover, the π-π stacking interaction with Phe168 (EL2) is not verified, as no hydrophobic interaction is detected. It is evident that an increased stabilization of adenosine occurred in the hA_1 AR-based model due to some crucial amino acids, i.e. Thr94 (3.36), Phe168 (EL2) and the not conserved residues Val169 (EL2) and Leu90 (3.32).

As for adenosine, all other agonists have been docked to any of the hA_3 ARs, and the best docking poses have been summarized in Video S1 (available as Supplementary Information).

Summarizing the docking results, all analyzed agonists were preferably fitted in the orthosteric binding site of the hA_1-based models of hA_3, as graphically shown in the correlation matrix of Figure 7, where the energetic contributions (electrostatic and van der Waals) assigned to the hA_1-based model are compared with the hA_{2A}-based one. The chromatic scale must be interpreted as follows: (a) the white color indicates favorable energetic contributions of the specific ligand (reported in the *y*-axis) for both hA_1-based model and hA_{2A}-based models (as for example calculated for ADO and MRS5127); (b) the orange color indicates unfavorable energetic contributions of the specific ligand for both hA_1-based model and hA_{2A}-based models; (c) the blue color indicates favorable energetic contributions of the specific ligand (reported in the *y*-axis) for the hA_1-based model and unfavorable for the hA_{2A}-based model (as for example calculated for MRS7110 and MRS5644); and, finally, (d) the red color indicates unfavorable energetic contributions of the specific ligand for the hA_1-based model and favorable for the hA_{2A}-based model. Moreover, the numerical value inside each cell describes, in logarithmic form, the ratio of the specific energy contribution calculated between the hA_1-based model and the

hA_{2A}-based reference model (see Equation (2), x and y respectively). From an interpretative point of view, if this value is more negative it means that this energetic contribution is much more favorable for the binding of the ligand versus the hA_1-based model compared to the hA_{2A}-based model, whereas when this value is more positive, the energetic contribution is much more favorable for the binding of the ligand versus the hA_{2A}-based model and compared to the hA_1-based model.

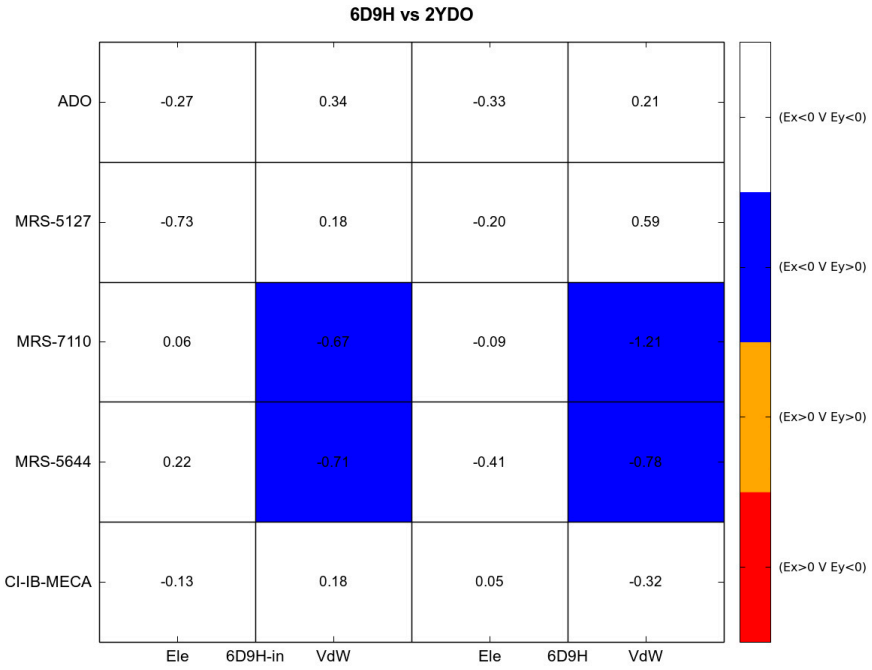

Figure 7. EM correlation matrix of energy contributions (electrostatic and van der Waals) for agonist poses (y-axis) obtained from the hA_1-based model with induce fit (6D9H-in) and without induce fit (6D9H), as compared to the reference model (2YDO).

From the analysis of the correlation matrix is deducible that all homology models, independently from the original template, are able to properly accommodate all selected agonists inside the orthosteric binding site of the hA_3 AR. However, in general, the energetic contributions for agonist-receptor interaction (electrostatic and/or van der Waals) indicates a higher stabilization in the hA_1-based model compared to a model based on A_{2A} structure, in particular for the agonists MRS7110 and MRS5644. Interestingly, when docked to the hA_1-based model, MRS-7110 achieves a very suitable accommodation for the 2-(4-aryl-1,2,3-triazolyl) substituent, in the proximity to both EL2 and TM2 (Figure 8). The 2-aryl-triazolyl derivative shows the conserved binding pattern of agonists and a ribosyl C2′-endo conformation. Conversely, MRS-5644 is partially displaced from the binding site. MRS-5644 presents a huge planar 2-arylethynyl substituent, which is thought to be responsible for selectivity towards the hA_3 AR. A favorable as possible accommodation of the substituent (without prohibitive sterical hindrance) must be determinant for hA_3 selectivity. None of the built models is able to predict the most suitable pose for this ligand, but the hA_1-based model can accommodate its analog MRS-7710, which shares a geometrically similar substituent in C2. This seems to be consistent with the evidence that the different conformation of the ELs and the TMs' shift observed for the hA_1 AR, as compared with the hA_{2A} subtype, leads to a different shape of the binding cavity. It is reasonable to assume that peculiar residues of the hA_3 AR sequence could further enhance this aspect, making the binding cavity more prone to locate even rigid bulky substituents, especially towards the TM2 and EL2. In order to explore this hypothesis, we built up another structure, based on the already obtained 6D9H-A_3 model, exploiting the MOE Induced Fit functionality in presence of the MRS-7110 ligand pose, whose coordinates had been previously superposed to the MRS-5644 pose (indeed, these ligands differ only for the respective functionalities in C2).

Docking results on the 6D9H-in A_3 AR model are visibly better: 5 out 5 poses are in line with the canonical binding interaction geometry of AR ligands, as shown in Video S2. Furthermore, interaction with Thr94 (3.36) and Asn250 (6.55) is significantly more stable for each ligand. Importantly, as hypothesized, MRS-5644 reaches a reliable orientation (Figure 8), with the 2-aryl-ethynyl substituent directed towards the TM2, on the side of EL2. Indeed, the model, as compared to the template 6D9H, shows a slight outward shift of the TMs 2, 3 and 7 upper regions, while an inward shift of the EL2 is observed (the measured Cα-RMSD is about 0.28 Å).

These results indicate that, ideally, the orthosteric site of the hA_3 AR active state may accommodate the peculiar substituents of selective agonists in the proximity of EL2 and TMs 2-3 through some expansion of the cavity, favored by the conserved and not conserved residues located in these regions, as Leu90 (3.32) [58], Gln167 (EL2) [59] and Thr94 (3.36).

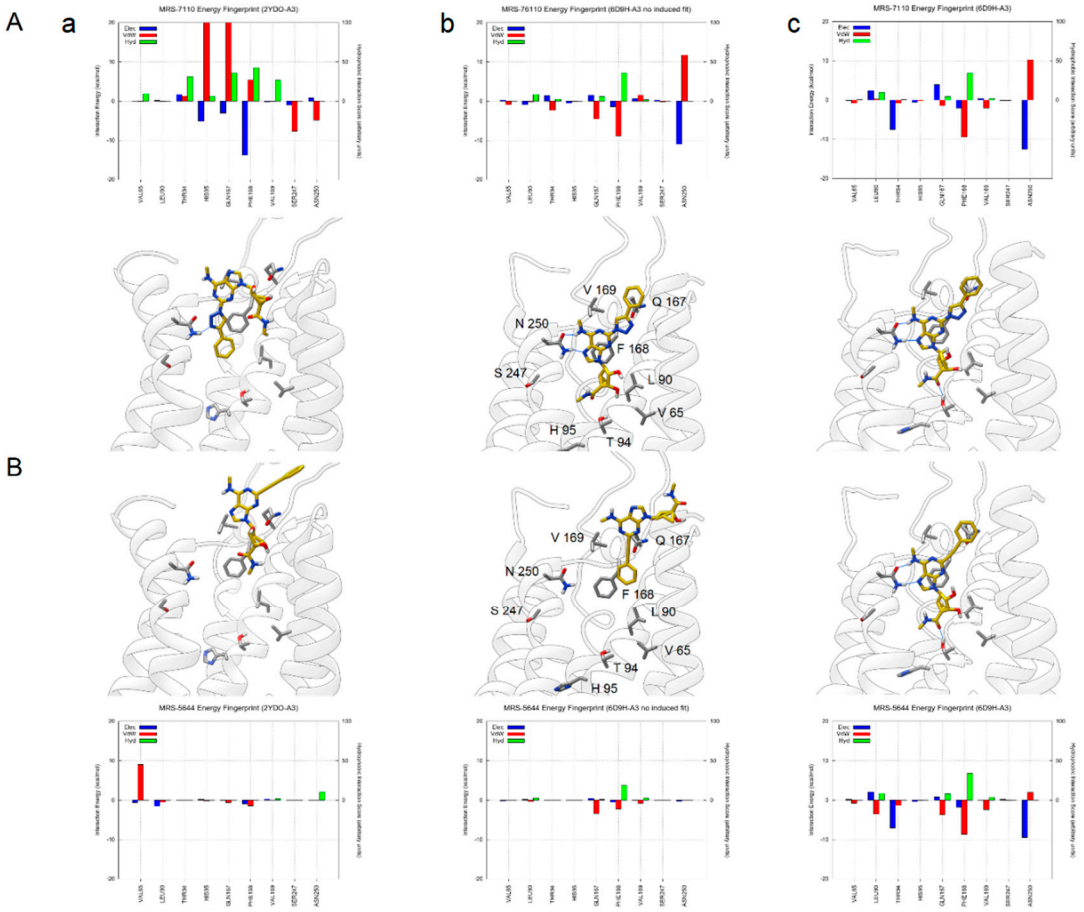

Figure 8. Per residue energy histograms and selected docking poses of MRS7110 (panel **A**) and MRS5644 (panel **B**) on either the hA_{2A} based model (**a**) or the hA_1 based models (**b**,**c**).

3.3. "Antagonist-driven" hA_3 AR Models

In contrast to the construction of the "agonist-driven" hA_3 AR models, in the case of "antagonist-driven" hA_3 AR, it has been decided to build up three different homology models, with two of these models using as templates the two hA_{2A} AR structures in complex with the antagonist ZM241385 (PDB codes: 3PWH and 5NM2, respectively), and the third one using as a template the hA_1 AR structure in complex with the antagonist DU1 (PDB code: 5UEN). As already anticipated, all "antagonist-driven" hA_3 AR models have been built up considering the sodium cation and its first hydration sphere as an integral part of the orthostatic site.

All other antagonists, as listed in Figure 3, have been docked in any of the three hA_3 ARs and the best docking poses have been summarized in Video S2 (available as Supplementary Information).

As for the comparison of agonists-driven docking results, even for antagonists the correlation matrix, shown in Figure 9, summarizes the energetic contributions (electrostatic and van der Waals) assigned to the hA_1-based and the hA_{2A} 5NM2 model compared to the hA_{2A} 3PWH model.

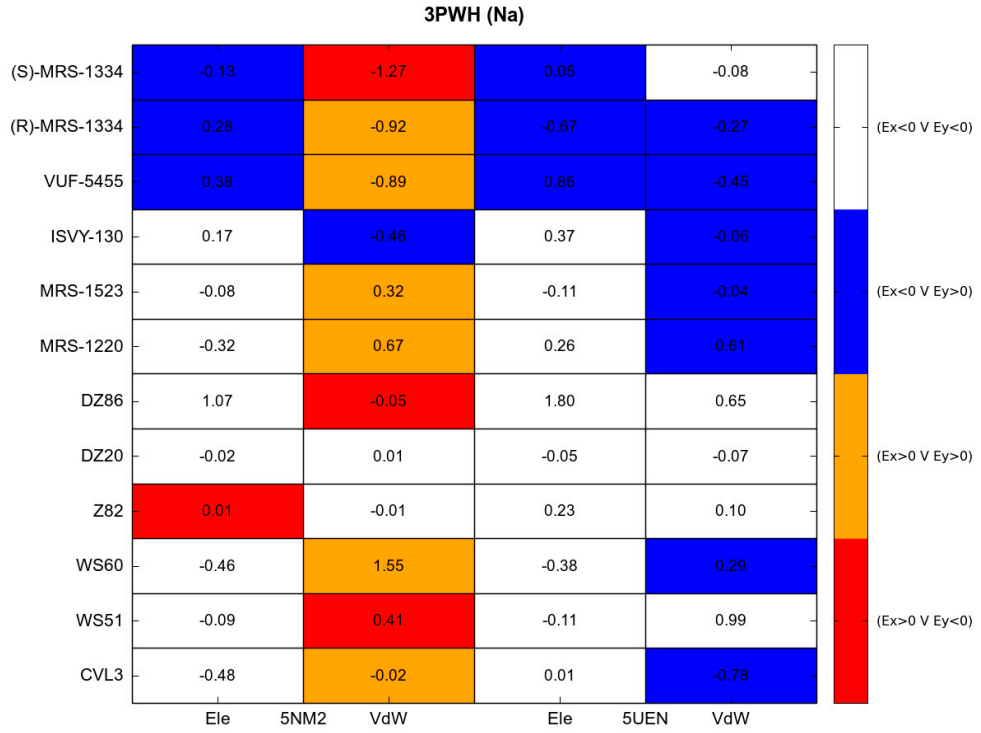

Figure 9. EM correlation matrix of energy contributions (electrostatic and van der Waals) for antagonists poses (*y*-axis), obtained from the hA_{2A}-based model (5NM2) and the hA_1-based model (5UEN), in comparison with the reference model (3PWH).

From the analysis of the correlation matrix, in this case, it is deducible that not all homology models equally stabilize the accommodation of the different antagonists in the orthosteric binding site of hA_3 AR. In particular, the energetic contributions for antagonist-receptor interaction (electrostatic and/or van der Waals) would seem to show a much higher stabilization in the hA_1-based model, compared to models based on both the A_{2A} structures, for several antagonists such as the highly selective 1,4-dihydropyridine derivative MRS-1334 (especially the *S*-enantiomers) or the isoquinoline VUF-5455.

As an example, the highly selective 1,4-dihydropyridine derivative MRS-1334 exists in two possible enantiomers, (*4R*) and (*4S*). It has been already demonstrated that the (*S*)-enantiomer is the main responsible for selectivity for this class of compounds [47]. The (*4S*)-enantiomer orients the *p*-nitrobenzyl substituent in the same direction of the aryl-ethynyl one, by intramolecular aromatic stacking interaction, conversely, the (*4R*)-enantiomer does to the top between TMs 1 and 7 (Figure 10). Enantiomers' poses differ mainly in the orientation of the ethyl ester substituent, up (4*S*) and down (4*R*), leading to different interactions as well. The (*4R*)-enantiomer shows very unfavorable interactions of the 2-phenyl moiety with the EL2 residue Val169. Conversely, the (*4S*)-enantiomer ethyl ester substituent contracts favorable interactions with Val169 and strong hydrophobic interactions with Phe168 (EL2). Hydrophobic interactions are established also with Val65 and Leu90. In general, the latter gives the main contribution to both enantiomers of MRS-1344 poses. These data are largely in favor of the (*4S*)-enantiomer, consistently with enantioselectivity observed. Asn250 (6.55) contribution is not determinant in this case, suggesting that excluding inevitable limitations of homology modeling, the *atypical* dihydropyridine scaffold in its *S*-configuration could be unable to engage hydrogen bonds

with Asn250 (6.55), except if we consider a rotation of the amidic side chain, i.e. the driving component of the final state may be mainly hydrophobic.

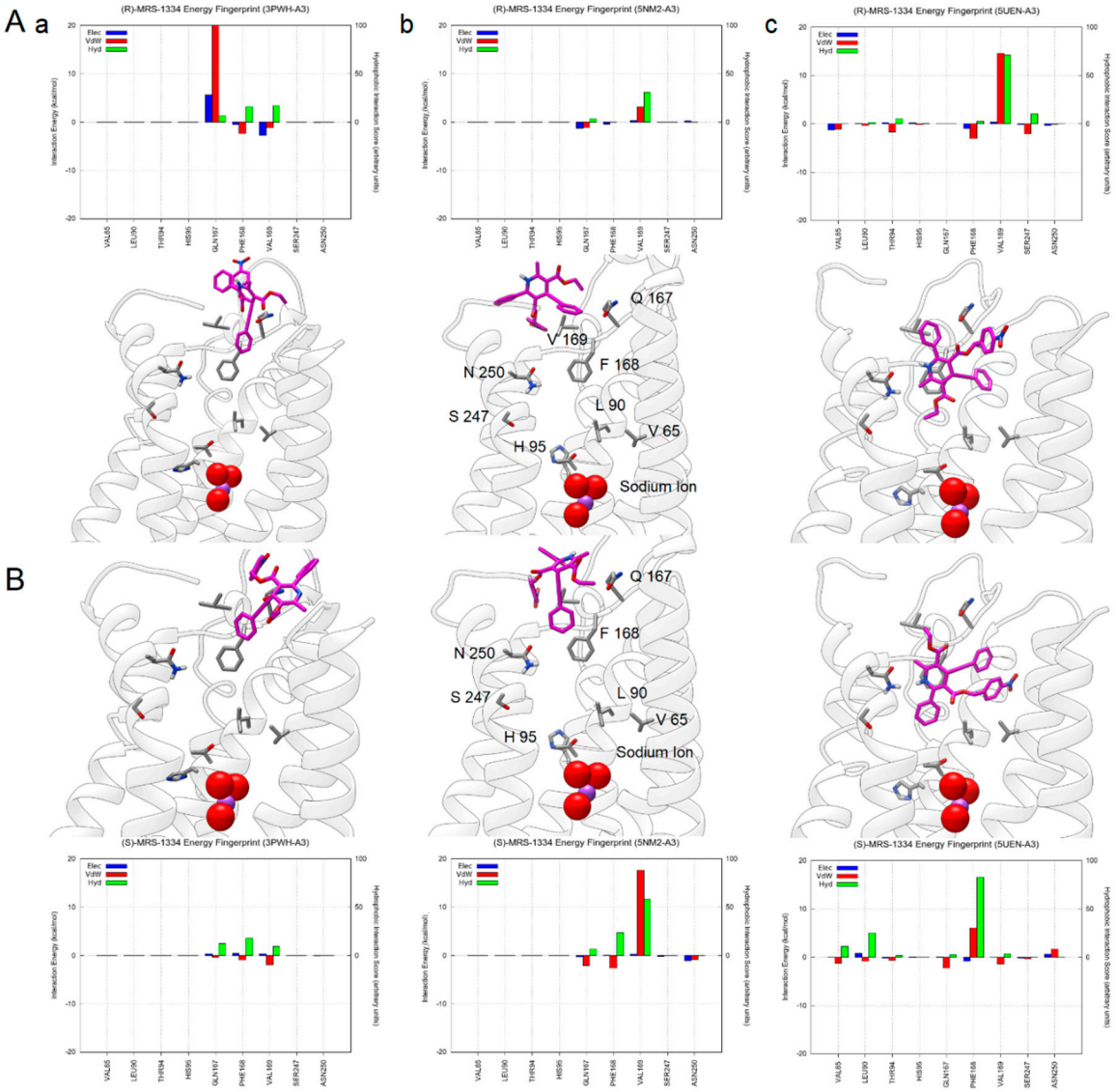

Figure 10. Per residue energy histograms and selected docking poses of (*4R*)-MRS1334 (panel **A**) and (*4S*)-MRS1334 (panel **B**) on either the hA2A-based models (**a**,**b**) or the hA_1-based model (**c**).

The potent antagonist VUF-5455, characterized by a not xanthinic scaffold as well, reveals a peculiar accommodation when docked to the hA_1 AR model. As shown in Figure 11 and Video S2, in this case, this antagonist establishes a highly favorable hydrogen bond with the canonical Asn250 (6.55), which is unfavorable instead in other models. Interaction with Leu90 (3.32), Phe168 (EL2) and Thr94 (3.36) is crucial, suggesting that also in this case these residues can play a major role in ligand recognition, creating highly selective hydrophobic locations for selective substituents.

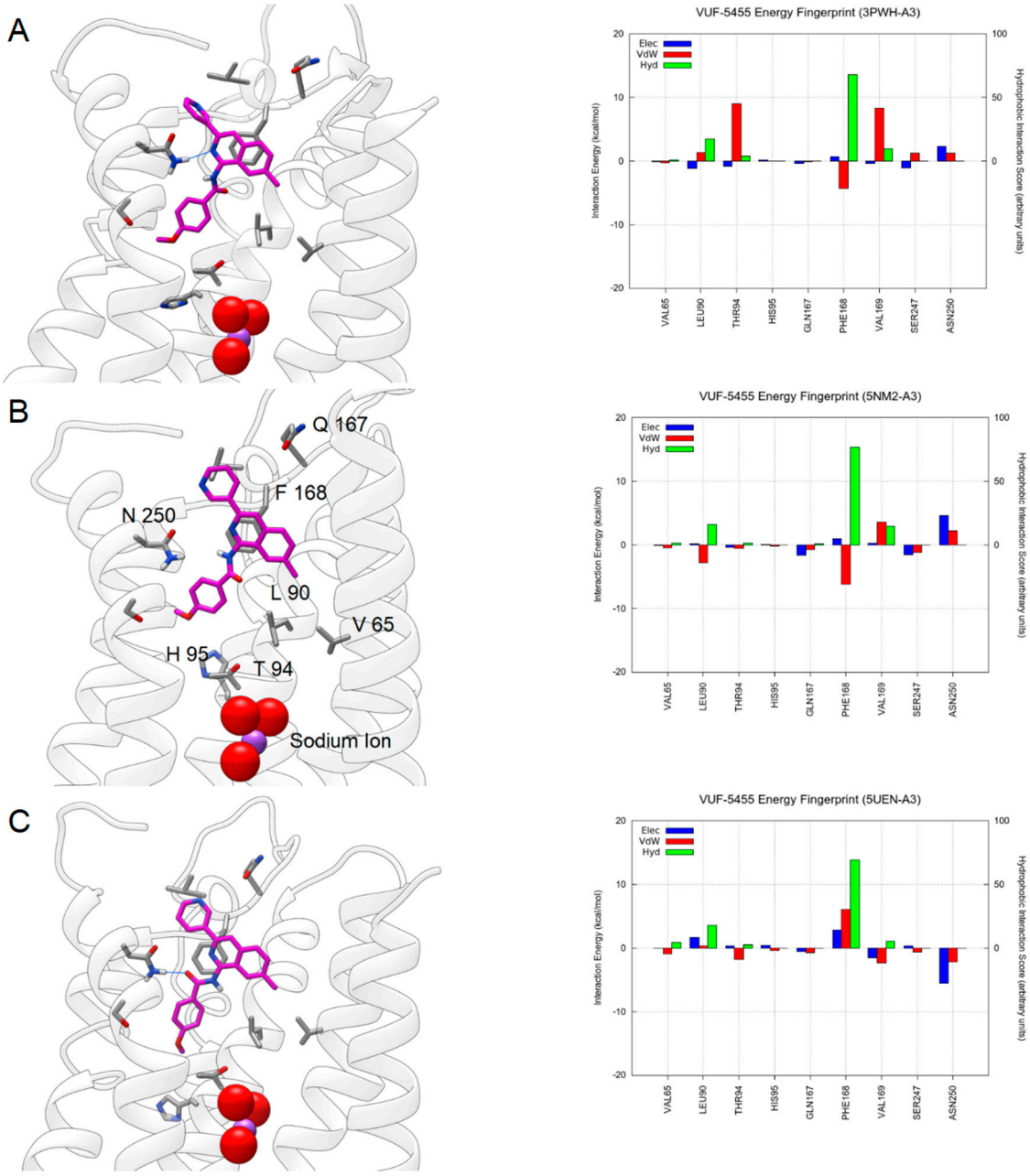

Figure 11. Per-residue energy histograms and selected docking poses of VUF-5455 on either the hA2A-based models (**A**,**B**) or the hA_1-based model (**C**).

4. Conclusions

On the basis of the results obtained from this preliminary study, it is possible to affirm that the human A_3 receptor model based on the crystallographic structure of the A_1 subtype can represent a valid alternative to the models conventionally used today based on the available A_{2A} structures, as supported by the comparative analysis of agonists and antagonists docking simulations on both models. A new series of molecular dynamics simulations (unbiased and supervised) are ongoing in our laboratory to accurately explore the time-dependent behavior of both models in terms of three-dimensional structure stability and in their capability to recognize both agonists and antagonists starting from an unbound state.

Supplementary Materials: The following are available online at http://www.mdpi.com/2076-3417/9/5/821/s1, Video S1: Agonist docking poses and energy fingerprint, Video S2: Antagonist docking poses and energy fingerprint.

Author Contributions: The overall work was driven within a strong joint framework between E.M. and S.M.

Funding: This research received no external funding.

Acknowledgments: S.M. is very grateful to Chemical Computing Group and Acellera for the scientific and technical partnerships. MMS lab gratefully acknowledges the support of NVIDIA Corporation with the donation of the Titan V GPU used for this research.

Conflicts of Interest: The authors declare no conflict of interest.

Abbreviations

AC	adenylate cyclase
ADO	adenosine
AR	adenosine receptor
BW-A522	3-(3-iodo-4-aminobenzyl)-8-(4-oxyacetate)-1-propylxanthine
CI-IB-MECA	Namodenoson
CVL3	N-{8-methyl-2-[1-(3-trifluoromethyl-benzyl)-1H-pyrazol-4-yl]-8H-pyrazolo[4,3-e][1,2,4]triazolo[1,5-c]pyrimidin-5-yl}-phenyl-acetamide
DZ20	2-furan-2-yl-5-methylamino-[1,2,4]triazolo[1,5-c]pyrimidine-8-carboxylic Acid Ethyl Ester
DZ86	2-Furan-2-yl-5-methylamino-[1,2,4]triazolo[1,5-c]pyrimidine-8-carboxylic acid 4-trifluoromethyl-benzylamide
EL	extracellular loop
Ele	electrostatic
GPCR	G protein-coupled receptor
h	human
Hyd	hydrophobic
IL	intracellular loop
-in	induced fit
I^{125}-APNEA	(N6-2-(4-amino-3iodophenyl)ethyladenosine)
MRS-1220	*N*-[9-chloro-2-(2-furanyl)[1,2,4]triazolo[1,5-c]quinazolin-5-yl]benzeneacetamide
MRS-1334	1,4-Dihydro-2-methyl-6-phenyl-4-(phenylethynyl)-3,5-pyridinedicarboxylic acid 3-ethyl-5-[(3-nitrophenyl)methyl] ester
MRS-5127	(1′R,2′R,3′S,4′R,5′S)-4′-[2-chloro-6-(3-iodobenzylamino)-purine]-2′,3′-O-dihydroxybicyclo-[3.1.0]hexane
MRS-5644	(1S,2R,3S,4R,5S)-2,3-Dihydroxy-N-methyl-4-(6-(methylamino)-2-(phenylethynyl)-9H-purin-9-yl)bicyclo[3.1.0]hexane-1-carboxamide
MRS-7110	(1S,2R,3S,4R,5S)-2,3dihydroxy-N-methyl-4-[6-(methylamino)-2-(4-phenyl-1H-1,2,3-triazol-1-yl)-5,9-dihydro-4H-purin-9-yl]bicyclo[3.1.0]hexane-1-carboxamide
NECA	5′-N-ethyl-carboxamidoadenosine
R	*R* configuration
r	rat
(*R*)-PIA	(*R*)-(-)-(N6)-1-phenyl-2-propyladenosine
RMSD	root mean square deviation
S	S configuration
SI	sequence identity
SS	sequence similarity
TM	transmembrane domain
vdW	van der Waals
VS	virtual screening
VUF-5455	4-methoxy-N-(7-methyl-3-(2-pyridinyl)-1-isoquinolinyl)benzamide
WS51	(*S*)-(2-Furan-2-yl-8-methyl-8H-pyrazolo[4,3-*e*][1,2,4]triazolo[1,5-*c*]pyrimidin-5-yl)-(1-phenylethyl)amine
WS60	Benzhydryl(2-furan-2-yl-8-methyl-8H-pyrazolo[4,3-*e*][1,2,4]triazolo[1,5-*c*]pyrimidin-5-yl)amine
Z82	N7-Benzyl-2-(furan-2-yl)-N5-isopropyl-[1,2,4]triazolo[1,5-*a*][1,3,5]triazine-5,7-diamine
ZM-241385	4-(2-(7-amino-2-(2-furyl)-(1,2,4)triazolo(2,3-*a*)-(1,3,5)triazin-5-yl-amino)ethyl)phenol

References

1. Kenneth, A.; Jacobson. *Adenosine Receptors in Health Disease, Handbook of Experimental Pharmacology*; Constance, N., Wilson, S., Mustafa, J., Eds.; Springer: Berlin, Germany, 2009.
2. Meyerhof, W.; Müller-Brechlin, R.; Richter, D. Molecular cloning of a novel putative G-protein coupled receptor expressed during rat spermiogenesis. *FEBS Lett.* **1991**, *284*, 155–160. [CrossRef]
3. Zhou, Q.Y.; Li, C.; Olah, M.E.; Johnson, R.A.; Stiles, G.L.; Civelli, O. Molecular cloning and characterization of an adenosine receptor: The A3 adenosine receptor. *Proc. Natl. Acad. Sci. USA* **1992**, *89*, 7432–7436. [CrossRef] [PubMed]
4. Borea, P.A.; Gessi, S.; Merighi, S.; Vincenzi, F.; Varani, K. Pharmacology of Adenosine Receptors: The State of the Art. *Physiol. Rev.* **2018**, *98*, 1591–1625. [CrossRef] [PubMed]
5. Janes, K.; Symons-Liguori, A.M.; Jacobson, K.A.; Salvemini, D. Identification of A3 adenosine receptor agonists as novel non-narcotic analgesics. *Br. J. Pharmacol.* **2016**, *173*, 1253–1267. [CrossRef] [PubMed]
6. Fishman, P.; Bar-Yehuda, S.; Liang, B.T.; Jacobson, K.A. Pharmacological and therapeutic effects of A3 adenosine receptor agonists. *Drug Discov. Today* **2012**, *17*, 359–366. [CrossRef] [PubMed]
7. Brown, R.A.; Spina, D.; Page, C.P. Adenosine receptors and asthma. *Br. J. Pharmacol.* **2008**, *153* (Suppl. 1), S446–S456. [CrossRef] [PubMed]
8. Wang, Z.; Do, C.W.; Avila, M.Y.; Peterson-Yantorno, K.; Stone, R.A.; Gao, Z.-G.; Joshi, B.; Besada, P.; Jeong, L.S.; Jacobson, K.A.; et al. Nucleoside-derived antagonists to A3 adenosine receptors lower mouse intraocular pressure and act across species. *Exp. Eye Res.* **2010**, *90*, 146–154. [CrossRef] [PubMed]
9. Ciancetta, A.; Sabbadin, D.; Federico, S.; Spalluto, G.; Moro, S. Advances in Computational Techniques to Study GPCR-Ligand Recognition. *Trends Pharmacol. Sci.* **2015**, *36*, 878–890. [CrossRef] [PubMed]
10. Deganutti, G.; Cuzzolin, A.; Ciancetta, A.; Moro, S. Understanding allosteric interactions in G protein-coupled receptors using Supervised Molecular Dynamics: A prototype study analysing the human A3 adenosine receptor positive allosteric modulator LUF6000. *Bioorg. Med. Chem.* **2015**, *23*, 4065–4071. [CrossRef] [PubMed]
11. Moro, S.; Morizzo, E.; Jacobson, K.A. Molecular modeling and reengineering of A3 adenosine receptors. In *A3 Adenosine Receptors from Cell Biology to Pharmacology and Therapeutics*; Borea, P.A., Ed.; Springer: Dordrecht, The Netherlands, 2010; pp. 149–161.
12. Sabbadin, D.; Moro, S. Supervised molecular dynamics (SuMD) as a helpful tool to depict GPCR-ligand recognition pathway in a nanosecond time scale. *J. Chem. Inf. Model.* **2014**, *54*, 372–376. [CrossRef] [PubMed]
13. Cuzzolin, A.; Sturlese, M.; Deganutti, G.; Salmaso, V.; Sabbadin, D.; Ciancetta, A.; Moro, S. Deciphering the Complexity of Ligand-Protein Recognition Pathways Using Supervised Molecular Dynamics (SuMD) Simulations. *J. Chem. Inf. Model.* **2016**, *56*, 687–705. [CrossRef] [PubMed]
14. Sabbadin, D.; Salmaso, V.; Sturlese, M.; Moro, S. Supervised Molecular Dynamics (SuMD) Approaches in Drug Design. *Methods Mol. Biol.* **2018**, *1824*, 287–298. [PubMed]
15. Draper-Joyce, C.J.; Khoshouei, M.; Thal, D.M.; Liang, Y.-L.; Nguyen, A.T.N.; Furness, S.G.B.; Venugopal, H.; Baltos, J.-A.; Plitzko, J.M.; Danev, R.; et al. Structure of the adenosine-bound human adenosine A1 receptor-Gi complex. *Nature* **2018**, *558*, 559–563. [CrossRef] [PubMed]
16. Glukhova, A.; Thal, D.M.; Nguyen, A.T.; Vecchio, E.A.; Jörg, M.; Scammells, P.J.; May, L.T.; Sexton, P.M.; Christopoulos, A. Structure of the Adenosine A1 Receptor Reveals the Basis for Subtype Selectivity. *Cell* **2017**, *168*, 867–877.e13. [CrossRef] [PubMed]
17. Chemical Computing Group—Citing MOE. Available online: https://www.chemcomp.com/Research-Citing_MOE.htm (accessed on 3 October 2016).
18. GOLD—The Cambridge Crystallographic Data Centre (CCDC). Available online: https://www.ccdc.cam.ac.uk/solutions/csd-discovery/components/gold/ (accessed on 12 March 2017).
19. GNUPLOT Homepage. Available online: http://gnuplot.sourceforge.net/ (accessed on 28 March 2018).
20. MarvinSketch. Available online: https://docs.chemaxon.com/display/docs/MarvinSketch+Home (accessed on 28 March 2018).
21. Pettersen, E.F.; Goddard, T.D.; Huang, C.C.; Couch, G.S.; Greenblatt, D.M.; Meng, E.C.; Ferrin, T.E. UCSF Chimera—A visualization system for exploratory research and analysis. *J. Comput. Chem.* **2004**, *25*, 1605–1612. [CrossRef] [PubMed]
22. Berman, H.M.; Westbrook, J.; Feng, Z.; Gilliland, G.; Bhat, T.N.; Weissig, H.; Shindyalov, I.N.; Bourne, P.E. The protein data bank. *Nucleic Acids Res.* **2000**, *28*, 235–242. [CrossRef] [PubMed]

23. Floris, M.; Sabbadin, D.; Ciancetta, A.; Medda, R.; Cuzzolin, A.; Moro, S. Implementing the "Best Template Searching" tool into Adenosiland platform. In *Silico Pharmacol 1*; Springer: Berlin, Germany, 2013.
24. Labute, P. Protonate3D: Assignment of ionization states and hydrogen coordinates to macromolecular structures. *Proteins* **2009**, *75*, 187–205. [CrossRef] [PubMed]
25. Labute, P. The generalized Born/volume integral implicit solvent model: Estimation of the free energy of hydration using London dispersion instead of atomic surface area. *J. Comput. Chem.* **2008**, *29*, 1693–1698. [CrossRef] [PubMed]
26. Wang, J.; Wolf, R.M.; Caldwell, J.W.; Kollman, P.A.; Case, D.A. Development and testing of a general amber force field. *J. Comput. Chem.* **2004**, *25*, 1157–1174. [CrossRef] [PubMed]
27. Weinert, T.; Olieric, N.; Cheng, R.; Brünle, S.; James, D.; Ozerov, D.; Gashi, D.; Vera, L.; Marsh, M.; Jaeger, K.; et al. Serial millisecond crystallography for routine room-temperature structure determination at synchrotrons. *Nat. Commun.* **2017**, *8*, 542. [CrossRef] [PubMed]
28. Halgren, T.A. Merck molecular force field. I. Basis, form, scope, parameterization, and performance of MMFF94. *J. Comput. Chem.* **1996**, *17*, 490–519. [CrossRef]
29. Stewart, J.J.P. Optimization of parameters for semiempirical methods I. Method. *J. Comput. Chem.* **1989**, *10*, 209–220. [CrossRef]
30. Bairoch, A.; Apweiler, R. The SWISS-PROT protein sequence database: Its relevance to human molecular medical research. *J. Mol. Med.* **1997**, *75*, 312–316. [PubMed]
31. Fredholm, B.B. Adenosine, adenosine receptors and the actions of caffeine. *Pharmacol. Toxicol.* **1995**, *76*, 93–101. [CrossRef] [PubMed]
32. Kim, H.O.; Ji, X.D.; Siddiqi, S.M.; Olah, M.E.; Stiles, G.L.; Jacobson, K.A. 2-Substitution of N6-benzyladenosine-5′-uronamides enhances selectivity for A3 adenosine receptors. *J. Med. Chem.* **1994**, *37*, 3614–3621. [CrossRef] [PubMed]
33. Jacobson, K.A.; Park, K.S.; Jiang, J.L.; Kim, Y.C.; Olah, M.E.; Stiles, G.L.; Ji, X.D. Pharmacological characterization of novel A3 adenosine receptor-selective antagonists. *Neuropharmacology* **1997**, *36*, 1157–1165. [CrossRef]
34. Tosh, D.K.; Finley, A.; Paoletta, S.; Moss, S.M.; Gao, Z.-G.; Gizewski, E.T.; Auchampach, J.A.; Salvemini, D.; Jacobson, K.A. In vivo phenotypic screening for treating chronic neuropathic pain: Modification of C2-arylethynyl group of conformationally constrained A3 adenosine receptor agonists. *J. Med. Chem.* **2014**, *57*, 9901–9914. [CrossRef] [PubMed]
35. Tosh, D.K.; Deflorian, F.; Phan, K.; Gao, Z.-G.; Wan, T.C.; Gizewski, E.; Auchampach, J.A.; Jacobson, K.A. Structure-guided design of A(3) adenosine receptor-selective nucleosides: Combination of 2-arylethynyl and bicyclo[3.1.0]hexane substitutions. *J. Med. Chem.* **2012**, *55*, 4847–4860. [CrossRef] [PubMed]
36. Tosh, D.K.; Paoletta, S.; Chen, Z.; Crane, S.; Lloyd, J.; Gao, Z.-G.; Gizewski, E.T.; Auchampach, J.A.; Salvemini, D.; Jacobson, K.A. Structure-Based Design, Synthesis by Click Chemistry and in Vivo Activity of Highly Selective A3 Adenosine Receptor Agonists. *MedChemComm* **2015**, *6*, 555–563. [CrossRef] [PubMed]
37. Auchampach, J.A.; Gizewski, E.T.; Wan, T.C.; de Castro, S.; Brown, G.G.; Jacobson, K.A. Synthesis and pharmacological characterization of [(125)I]MRS5127, a high affinity, selective agonist radioligand for the A3 adenosine receptor. *Biochem. Pharmacol.* **2010**, *79*, 967–973. [CrossRef] [PubMed]
38. Federico, S.; Redenti, S.; Sturlese, M.; Ciancetta, A.; Kachler, S.; Klotz, K.-N.; Cacciari, B.; Moro, S.; Spalluto, G. The Influence of the 1-(3-Trifluoromethyl-Benzyl)-1H-Pyrazole-4-yl Moiety on the Adenosine Receptors Affinity Profile of Pyrazolo[4,3-e][1,2,4]Triazolo[1,5-c]Pyrimidine Derivatives. *PLoS ONE* **2015**, *10*, e0143504. [CrossRef] [PubMed]
39. Federico, S.; Ciancetta, A.; Porta, N.; Redenti, S.; Pastorin, G.; Cacciari, B.; Klotz, K.N.; Moro, S.; Spalluto, G. Scaffold decoration at positions 5 and 8 of 1,2,4-triazolo[1,5-c]pyrimidines to explore the antagonist profiling on adenosine receptors: A preliminary structure-activity relationship study. *J. Med. Chem.* **2014**, *57*, 6210–6225. [CrossRef] [PubMed]
40. Federico, S.; Ciancetta, A.; Porta, N.; Redenti, S.; Pastorin, G.; Cacciari, B.; Klotz, K.N.; Moro, S.; Spalluto, G. 5,7-Disubstituted-[1,2,4]triazolo[1,5-a][1,3,5]triazines as pharmacological tools to explore the antagonist selectivity profiles toward adenosine receptors. *Eur. J. Med. Chem.* **2016**, *108*, 529–541. [CrossRef] [PubMed]
41. Federico, S.; Ciancetta, A.; Sabbadin, D.; Paoletta, S.; Pastorin, G.; Cacciari, B.; Klotz, K.N.; Moro, S.; Spalluto, G. Exploring the directionality of 5-substitutions in a new series of 5-alkylaminopyrazolo[4,3-e]1,2,4-triazolo[1,5-c]pyrimidine as a strategy to design novel human a(3) adenosine receptor antagonists. *J. Med. Chem.* **2012**, *55*, 9654–9668. [CrossRef] [PubMed]

42. Federico, S.; Margiotta, E.; Salmaso, V.; Pastorin, G.; Kachler, S.; Klotz, K.-N.; Moro, S.; Spalluto, G. [1,2,4]Triazolo[1,5-c]pyrimidines as adenosine receptor antagonists: Modifications at the 8 position to reach selectivity towards A3 adenosine receptor subtype. *Eur. J. Med. Chem.* **2018**, *157*, 837–851. [CrossRef] [PubMed]
43. Kim, Y.C.; Ji, X.D.; Jacobson, K.A. Derivatives of the triazoloquinazoline adenosine antagonist (CGS15943) are selective for the human A3 receptor subtype. *J. Med. Chem.* **1996**, *39*, 4142–4148. [CrossRef] [PubMed]
44. Li, A.H.; Moro, S.; Melman, N.; Ji, X.D.; Jacobson, K.A. Structure-activity relationships and molecular modeling of 3, 5-diacyl-2,4-dialkylpyridine derivatives as selective A3 adenosine receptor antagonists. *J. Med. Chem.* **1998**, *41*, 3186–3201. [CrossRef] [PubMed]
45. Gao, Z.G.; Van Muijlwijk-Koezen, J.E.; Chen, A.; Müller, C.E.; Ijzerman, A.P.; Jacobson, K.A. Allosteric modulation of A(3) adenosine receptors by a series of 3-(2-pyridinyl)isoquinoline derivatives. *Mol. Pharmacol.* **2001**, *60*, 1057–1063. [CrossRef] [PubMed]
46. Xie, R.; Li, A.H.; Ji, X.D.; Melman, N.; Olah, M.E.; Stiles, G.L.; Jacobson, K.A. Selective A(3) adenosine receptor antagonists: Water-soluble 3, 5-diacyl-1,2,4-trialkylpyridinium salts and their oxidative generation from dihydropyridine precursors. *J. Med. Chem.* **1999**, *42*, 4232–4238. [CrossRef] [PubMed]
47. Jiang, J.; Li, A.H.; Jang, S.Y.; Chang, L.; Melman, N.; Moro, S.; Ji, X.; Lobkovsky, E.B.; Clardy, J.C.; Jacobson, K.A. Chiral resolution and stereospecificity of 6-phenyl-4-phenylethynyl- 1,4-dihydropyridines as selective A(3) adenosine receptor antagonists. *J. Med. Chem.* **1999**, *42*, 3055–3065. [CrossRef] [PubMed]
48. Ciancetta, A.; Jacobson, K. Structural Probing and Molecular Modeling of the A3 Adenosine Receptor: A Focus on Agonist Binding. *Molecules* **2017**, *22*, 449. [CrossRef] [PubMed]
49. Ciancetta, A.; Cuzzolin, A.; Moro, S. Alternative quality assessment strategy to compare performances of GPCR-ligand docking protocols: The human adenosine A_{2A} receptor as a case study. *J. Chem. Inf. Model.* **2014**, *54*, 2243–2254. [CrossRef] [PubMed]
50. Cuzzolin, A.; Sturlese, M.; Malvacio, I.; Ciancetta, A.; Moro, S. DockBench: An integrated informatic platform bridging the gap between the robust validation of docking protocols and virtual screening simulations. *Molecules* **2015**, *20*, 9977–9993. [CrossRef] [PubMed]
51. Margiotta, E.; Deganutti, G.; Moro, S. Could the presence of sodium ion influence the accuracy and precision of the ligand-posing in the human A2A adenosine receptor orthosteric binding site using a molecular docking approach? Insights from Dockbench. *J. Comput. Aided Mol. Des.* **2018**, *32*, 1337–1346. [CrossRef] [PubMed]
52. RDKit: Cheminformatics and Machine Learning Software. Available online: http://www.rdkit.org (accessed on 28 March 2018).
53. Mencoder. Available online: http://www.mplayerhq.hu/design7/projects.html (accessed on 28 March 2018).
54. Martinelli, A.; Ortore, G. Molecular Modelling of adenosine receptors. *Meth. Enzymol.* **2013**, *522*, 37–59. [CrossRef] [PubMed]
55. Piirainen, H.; Ashok, Y.; Nanekar, R.T.; Jaakola, V.-P. Structural features of adenosine receptors: From crystal to function. *Biochim. Biophys. Acta (BBA)-Biomembr. Adenosine Recept.* **2011**, *1808*, 1233–1244. [CrossRef] [PubMed]
56. Belardinelli, L.; Pelleg, A. *Adenosine and Adenine Nucleotides: From Molecular Biology to Integrative Physiology*; Springer Science & Business Media: Berlin, Germany, 1995.
57. Fiser, A. Template-Based Protein Structure Modeling. *Methods Mol. Biol.* **2010**, *673*, 73–94. [PubMed]
58. Campbell, N.G.; Zhu, C.-B.; Lindler, K.M.; Yaspan, B.L.; Kistner-Griffin, E.; Hewlett, W.A.; Tate, C.G.; Blakely, R.D.; Sutcliffe, J.S. Rare coding variants of the adenosine A3 receptor are increased in autism: On the trail of the serotonin transporter regulome. *Mol. Autism* **2013**, *4*, 28. [CrossRef] [PubMed]
59. Gao, Z.-G.; Chen, A.; Barak, D.; Kim, S.-K.; Müller, C.E.; Jacobson, K.A. Identification by Site-directed Mutagenesis of Residues Involved in Ligand Recognition and Activation of the Human A3 Adenosine Receptor. *J. Biol. Chem.* **2002**, *277*, 19056–19063. [CrossRef] [PubMed]